Self-Impedance-Matched Hall-Effect Gyrators and Circulators

S. Bosco,[1,3,*] F. Haupt,[1,3] and D. P. DiVincenzo[1,2,3,†]

[1]*Institute for Quantum Information, RWTH Aachen University, D-52056 Aachen, Germany*

[2]*Peter Grünberg Institute, Theoretical Nanoelectronics, Forschungszentrum Jülich, D-52425 Jülich, Germany*

[3]*Jülich-Aachen Research Alliance (JARA), Fundamentals of Future Information Technologies, D-52425 Jülich, Germany*

(Received 27 October 2016; revised manuscript received 31 January 2017; published 27 February 2017)

We present a model study of an alternative implementation of a two-port Hall-effect microwave gyrator. Our setup involves three electrodes, one of which acts as a common ground for the others. Based on the capacitive-coupling model of Viola and DiVincenzo, we analyze the performance of the device and we predict that ideal gyration can be achieved at specific frequencies. Interestingly, the impedance of the three-terminal gyrator can be made arbitrarily small for certain coupling strengths, so that no auxiliary impedance matching is required. Although the bandwidth of the device shrinks as the impedance decreases, it can be improved by reducing the magnetic field; it can be realistically increased up to 150 MHz at 50 Ω by working at the filling factor $\nu = 10$. We also examine the effects of the parasitic capacitive coupling between electrodes and we find that, although, in general, they strongly influence the response of device, their effect is negligible at low impedance. Finally, we analyze an interferometric implementation of a circulator, which incorporates the gyrator in a Mach-Zender–like construction. Perfect circulation in both directions can be achieved, depending on frequency and on the details of the interferometer.

DOI: 10.1103/PhysRevApplied.7.024030

I. INTRODUCTION

Nonreciprocal devices such as gyrators and circulators are key components in modern microwave engineering. Circulators, for example, are crucial for reducing thermal noise and for directing signals in superconducting circuits [1,2]. An ideal circulator is a three-port device that cyclically routes a signal to the next port. One conventional implementation of circulators exploits the electromagnetic Faraday effect in ferromagnets [3,4]. Although excellent circulation can be obtained, this setup has a fundamental scalability limit, which sets the minimal size of the device to the order of centimeters. Alternative, more compact designs rely on active components, typically operational amplifiers [5], whose performance is currently not guaranteed at cryogenic temperatures.

In this work, we will at first focus on gyrators. An ideal gyrator is a two-port device that adds a phase shift of π between forward- and backward-propagating signals: this behavior is captured by a scattering (S) matrix of the form [6]

$$S = e^{i\varphi}\begin{pmatrix} 0 & -1 \\ 1 & 0 \end{pmatrix}. \tag{1}$$

Recently, Viola and DiVincenzo (VD) [7] revisited the old idea of obtaining nonreciprocity by exploiting the Hall effect (HE). Previous studies of Hall-effect gyrators focused on Ohmic contacts between the external metal electrodes and the Hall bar [8,9] and showed that the device has, in this case, an input resistance larger than the gyration resistance, which severely degrades the performance. By contrast, VD considered a Hall bar *capacitively* coupled to external electrodes, and they predicted that it could behave as an optimal nonreciprocal device in specific ranges of frequency. Motivated by this work, an early experimental realization of a HE circulator was attempted by Mahoney *et al.* (MEA) [10]. Although this experiment showed the potential of this alternative setup, it also pointed out a number of engineering challenges to be faced. In particular, MEA focused on the Carlin construction of a circulator [7,11,12], and, in this case, the performance of the device is strongly affected by the high impedance mismatch between the Hall conductor and the external microwave circuit and by the parasitic coupling between the electrodes. A model study of these effects in that case is extensively discussed in Ref. [13].

In this work, we analyze an alternative setup for HE gyrators and circulators that is highly insensitive to impedance mismatch and parasitics. VD proposed a bipolarly driven four-terminal gyrator, where each pair of opposite electrodes is driven by identical voltage signals, with opposing signs. Here, we consider instead a three-terminal gyrator, with one terminal acting as common ground. Not only is this setup experimentally easier to implement, but we find that, for certain coupling strengths,

*bosco@physik.rwth-aachen.de
†d.divincenzo@fz-juelich.de

it also exhibits a very interesting self-matching property: its impedance can be made arbitrarily small, so that no additional impedance matching is required. We predict that, as the impedance decreases, unwanted effects due to parasitics will become negligible on one hand and, on the other hand, the frequency range (bandwidth) within which the device works will shrink. However, we also find that the bandwidth can be improved by lowering the magnetic field, and that, for realistic device parameters, it can be sufficiently large for several applications, e.g., approximately 150 MHz at filling factor $\nu = 10$ and external impedance 50 Ω.

Finally, we analyze an alternative implementation of a circulator, which incorporates the three-terminal HE gyrator into a Mach-Zender–like interferometer. We find that the quality and the direction of the circulation are crucially related to the details of the interferometer. Specifically, to have ideal circulation in the smallest possible setup, i.e., when all arms of the interferometer are very short, directional couplers with both π and $\pi/2$ phase shifts are required. In this case, the size of the circulator is mainly limited by the size of the directional couplers, which are typically implemented on chip in $\lambda/4$ ring structures, and which can be miniaturized to λ/N, $N \approx 20$ by standard microwave-engineering techniques [14].

II. THREE-TERMINAL GYRATOR

A. Basic analysis

We analyze the performance of the HE gyrator composed of a two-dimensional conductor capacitively coupled to three perfectly conducting electrodes, as shown in Fig. 1.

To attain nonreciprocity, a homogeneous magnetic field is applied perpendicularly to the plane of the conductor.

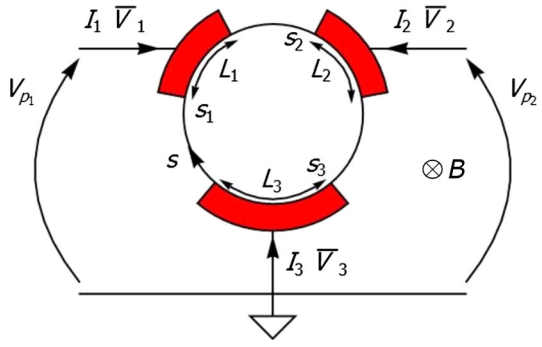

FIG. 1. Three-terminal gyrator. Three electrodes are capacitively coupled to a Hall bar whose boundary is parametrized by s. The capacitances are shown in red, and their position along the perimeter is determined by their starting coordinate s_i and by the length L_i of the electrodes. A homogeneous magnetic field is applied perpendicularly to the conductor, and it points inward. The device behaves as a two-port gyrator when the voltage of two electrodes is measured with respect to the last one, which acts as a common ground. The convention of currents and voltages is shown in the plot.

The charge carriers are then subjected to the Lorentz force, and the current-density vector is rotated by a fixed (Hall) angle θ_H with respect to the electric-field vector.

In this work, we focus only on the fully developed quantum Hall effect [15]—i.e., when the material conductance is at a quantum Hall plateau and the diagonal components of the conductivity tensor vanish. This set of conditions implies that the current in the two-dimensional conductor is perpendicular to the electric field ($\theta_H \to \pi/2$) and that the device is lossless. The effect of a finite diagonal conductivity is analyzed in Refs. [7,13]; in this case, the device is lossy, but for a sufficiently high magnetic field, θ_H does not vary much from the limiting value $\pi/2$ and the losses are small.

To model the device, we follow VD and begin by computing the electric potential V inside the Hall bar. This potential has to satisfy the Laplace equation,

$$\nabla^2 V(x, y) = 0, \tag{2}$$

with boundary conditions accounting for the applied magnetic field and the coupling to the electrodes. The work of VD showed that, in the quantum Hall regime, the boundary conditions on V reduce to the one-dimensional closed differential equation

$$-\sigma \partial_s V(s, \omega) = i\omega c(s)[\bar{V}(\omega) - V(s, \omega)] \tag{3}$$

in the perimeter coordinate s. Here, $\bar{V}$ is the voltage drive applied at the terminals and $\sigma = \nu e^2/h$ is the quantum Hall conductivity at filling factor ν (e is the electron charge and h is the Planck constant). The phenomenological function $c(s)$ has a dimension of capacitance per unit length, and it accounts for the capacitive coupling to the external metal electrodes. When the capacitors are much longer than the gap between them, one can neglect fringing fields and $c(s)$ is well approximated by the stepwise function

$$c(s) = \begin{cases} c_1 & s_1 < s < s_1 + L_1 \\ c_2 & s_2 < s < s_2 + L_2 \\ c_3 & s_3 < s < s_3 + L_3 \\ 0 & \text{otherwise.} \end{cases} \tag{4}$$

The parameters c_i should incorporate both classical electrostatic-coupling and quantum-capacitance effects. We will report separately [16] on a microscopic calculation, based on the RPA, that gives the driven response of the 2D Hall conductor; this calculation incorporates details of the edge-conductor geometry, of the band structure and of the edge-confinement physics of the 2D material. For both heterostructure and graphene models, we confirm that the simple approximations of the VD theory give results in agreement with the RPA calculation in many situations of interest.

A peculiar feature of the quantum Hall limit is that the boundary potential $V(s,\omega)$ depends only on the edge dimension, and thus the VD model captures the behavior of Hall bars of arbitrary shapes. Moreover, as VD pointed out, in this case, $V(s,\omega)$ fully determines the dynamics of the potential inside the material, and all of the interesting parameters characterizing the device response can be computed from it. For example, the current in the ith electrode is simply [7]

$$I_i(\omega) = \sigma[V(s = s_i,\omega) - V(s = s_i + L_i,\omega)]. \quad (5)$$

To study a two-port gyrator, we define the port voltages and currents as

$$V_{p_1} = \bar{V}_1 - \bar{V}_3, \qquad I_{p_1} = I_1, \quad (6a)$$

$$V_{p_2} = \bar{V}_2 - \bar{V}_3, \qquad I_{p_2} = I_2; \quad (6b)$$

see Fig. 1. Combining Eqs. (3), (5), and (6), we find the port-admittance matrix Y_p and, by using the standard relation [6]

$$S = -\left(Y_p + \frac{1}{Z_0}\mathcal{I}\right)^{-1}\left(Y_p - \frac{1}{Z_0}\mathcal{I}\right), \quad (7)$$

we can evaluate the S parameters of the device. In Eq. (7), $\mathcal{I}$ is the identity matrix and Z_0 is the characteristic impedance of the external microwave circuit, typically 50 Ω.

For simplicity, we now focus on a symmetric situation, with $C \equiv c_1L_1 = c_2L_2$, and we introduce the dimensionless parameter $r \equiv c_3L_3/C$, which characterizes the strength of the coupling to the ground electrode with respect to the others. Substituting Y_p into Eq. (7), we find that the scattering matrix assumes the form

$$S = \begin{pmatrix} S_{11} & S_{21}e^{i\Omega r} \\ S_{21} & S_{11} \end{pmatrix}, \quad (8)$$

where Ω is the dimensionless frequency of the signal defined by

$$\Omega \equiv \omega C/\sigma. \quad (9)$$

The explicit expressions for S_{11} and S_{21} are shown in the Appendix.

From Eq. (8), it follows that maximal nonreciprocity is obtained at the frequencies

$$\Omega_n = \frac{\pi}{r}(2n+1), \quad \text{with} \quad n \in \mathbb{N}. \quad (10)$$

Condition (10) is necessary but not sufficient to achieve ideal gyration. In fact, an ideal gyrator needs to be both antireciprocal and reflectionless, with $S_{11} = S_{22} = 0$. Hence, to quantitatively analyze the device, we introduce

$$\Delta \equiv \frac{1}{2}|S_{21} - S_{12}| \le 1, \quad (11a)$$

$$\varphi \equiv \arg(S_{21} - S_{12}). \quad (11b)$$

Specifically, Δ characterizes the gyrator performance since the unitarity of the S matrix guarantees that equality in Eq. (11a) is attained only for ideal gyrators. The overall phase factor φ is crucial for fixing the parameters of the interferometric implementation of a circulator.

In general, the reflection coefficients strongly depend on the impedance mismatch between the Hall bar and the external system. To characterize the impedance mismatch, we define the dimensionless parameter $\alpha \equiv 2\sigma Z_0$.

First, we focus on antireciprocal devices. Figure 2 shows how Δ is influenced by α and r at the first gyration frequency, $\Omega = \Omega_0 \equiv \pi/r$. We note that, for all values of the mismatch parameter $\alpha \le 1$, there is a value of r at which perfect gyration is attained. This consideration indicates that the impedance of the HE gyrator can be made arbitrarily small by choosing an appropriate ratio between the coupling strength of the electrodes. Specifically, it is straightforward to show that the condition $\Delta(\Omega_n) = 1$ holds when r and α are related by the transcendental equation

$$\cos\left(\frac{\pi}{r}(2n+1)\right) = 1 - \frac{1}{1-\alpha^2/2}. \quad (12)$$

This striking self-matching property is a new feature of our three-terminal construction, which can be exploited to engineer compact devices not requiring external impedance matching. From an experimental point of view, the case $\alpha \ll 1$ is of the utmost importance since, in the quantum

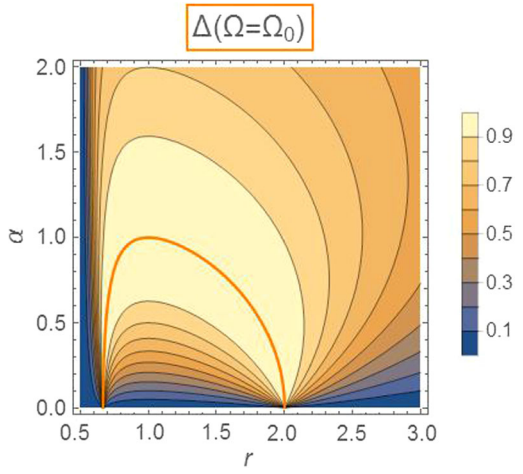

FIG. 2. Dependence of Δ on $r \equiv c_3L_3/(c_1L_1)$ and $\alpha \equiv 2\sigma Z_0$ evaluated at the first gyration frequency, $\Omega_0 \equiv \pi/r$. Good gyration requires Δ to be near 1. Along the orange line, the value $\Delta = 1$ is exactly attained, giving perfect gyration.

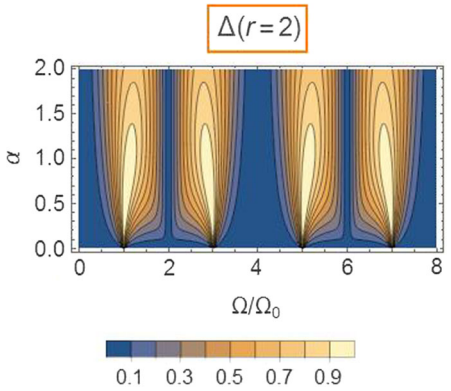

FIG. 3. Δ as a function of $\alpha \equiv 2\sigma Z_0$ and of the dimensionless frequency Ω, normalized by the first gyration frequency, $\Omega_0 \equiv \pi/r$. The plot shows the result when $r \equiv c_3 L_3/(c_1 L_1) = 2$, which corresponds to the self-matched case.

Hall regime, $\alpha \approx 0.004\nu$ at 50 Ω. If we expand condition (12) for a small α, we obtain the simple formula

$$r = \frac{2(2n+1)}{2(m-n)-1} + O(\alpha^2), \quad \text{with} \quad n, m \in \mathbb{N}, \tag{13}$$

and $m \geq n+1$.

It is now worth analyzing in more detail the frequency response of the self-matched construction. Figure 3 shows Δ as a function of α and Ω when $r = 2$. First of all, it is interesting to note that the response is periodic in Ω, with the period 2π. Moreover, although, strictly speaking, perfect gyration is achieved only at $\alpha \to 0$ and $\Omega = \Omega_n$, excellent performance is seen in a broader range of parameters.

To quantitatively analyze this range, we set the threshold defining a good device to $\Delta = 0.9$ and we introduce the bandwidth (BW) of the device as the dimensionless frequency range $\Delta\Omega$, for which $\Delta \geq 0.9$. Figure 4 shows the dependence of $\Delta\Omega$ on α. Increasing α from zero, the BW of the gyrator increases approximately linearly with the slope $k \approx 0.49$ until the maximal BW is obtained at $\alpha \approx 1$, which corresponds to the perfectly matched limit in Ref. [7].

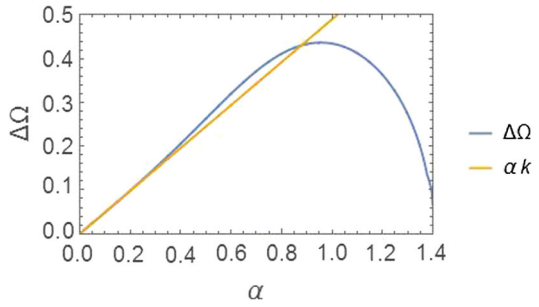

FIG. 4. Dependence of $\Delta\Omega$ on α in the self-matched case with $r = 2$. The BW increases up to $\alpha = 1$ and then it decreases abruptly. In the interesting impedance regime, $\alpha \lesssim 0.4$, the increase of the BW is, to good approximation, linear, with the slope $k \approx 0.49$.

Using a realistic capacitance value of $C = 50$ fF and for $r = 2$, one can implement devices working at frequencies $\omega_n \approx 1.2\nu(2n+1)$ GHz, with the bandwidth $\Delta\omega \approx 1.5\nu^2$ MHz at $Z_0 = 50\ \Omega$. Note that by increasing the filling factor ν, the gyration frequency increases linearly, while the BW increases quadratically. Hence, by lowering the magnetic field, a bandwidth which is useful for several practical applications, e.g., equal approximately to 150 MHz at $\nu = 10$, can be easily reached.

B. Parasitic capacitances

Motivated by recent works—both theoretical and experimental [10,13]—we now include the effect of the parasitic capacitive coupling between electrodes, and we predict that, at low enough impedance, these effects are negligible. We consider the augmented network shown in Fig. 5. For simplicity, we assume the electrodes 1 and 2 to be placed symmetrically with respect to the third, such that two of the three parasitic capacitors are equal, $C_{p_1} = C_{p_3}$.

From a straightforward circuit analysis, since the parasitic channels are in parallel with the device, the admittance matrix of the augmented network Y_a is

$$Y_a = Y_p + Y_1 + Y_2, \tag{14}$$

with

$$Y_1 = i\omega C_{p_1} \mathcal{I}, \tag{15a}$$

$$Y_2 = i\omega C_{p_2} \begin{pmatrix} 1 & -1 \\ -1 & 1 \end{pmatrix}. \tag{15b}$$

The scattering parameters are then readily found by using Eq. (7).

To characterize the effect of the parasitic channels, we begin by analyzing the nonreciprocal behavior of the device. We find that the frequency that guarantees maximal

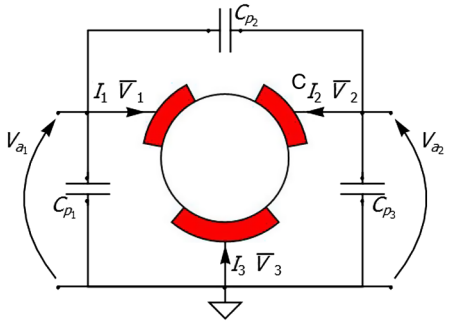

FIG. 5. Augmented network incorporating parasitic capacitive coupling between the three electrodes. The convention on port voltages V_a is shown.

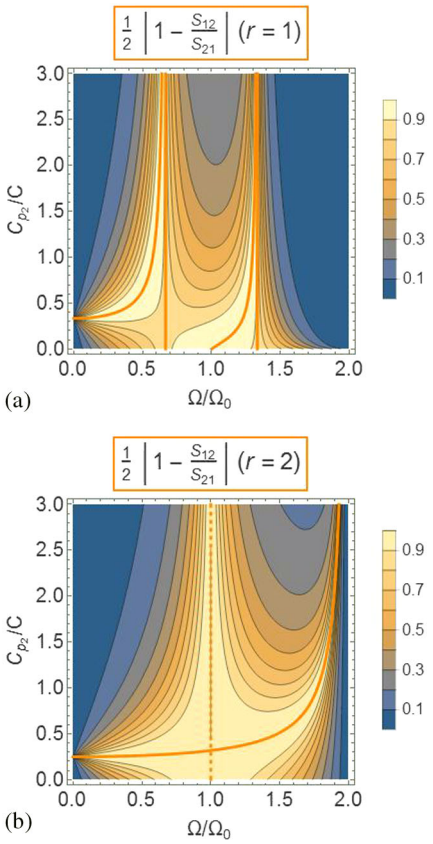

FIG. 6. Nonreciprocity contribution to Δ at different r's as a function of C_{p_2} and Ω/Ω_0. In (a), we use $r = 1$; in (b), $r = 2$. The ratio between the off-diagonal terms depends neither on α nor on C_{p_1}. The orange lines represent the maximally antireciprocal case, attained for $|1 - S_{12}/S_{21}|/2 = 1$. Specifically, the dashed line corresponds to condition (16a), while the solid line corresponds to condition (16b).

nonreciprocity is shifted depending on C_{p_2}. To examine this phenomenon, we study the quantity $|1 - S_{12}/S_{21}|/2$, which is equal to 1 only for antireciprocal devices. In Fig. 6, we show its dependence on Ω and C_{p_2} for two different values of r. The behavior observed in the figure is explained by considering that there are two different conditions that guarantee maximal antireciprocity:

$$r = \frac{2(2n+1)}{2(m-n)-1} \wedge \Omega = \Omega_n, \quad \text{or} \tag{16a}$$

$$\frac{C_{p_2}}{C} = \frac{2}{\Omega}\sin^2\left(\frac{\Omega}{2}\right)\cos\left(\frac{\Omega r}{2}\right)\csc\left(\frac{\Omega}{2}(r+2)\right), \tag{16b}$$

with Ω_n being the gyration frequencies in Eq. (10).

The former condition (16a) corresponds to the self-matching conditions for small α's in Eq. (13): as it does not depend on the parasitic capacitors, it explains the straight line in Fig. 6(b) at $\Omega = \Omega_0$. By contrast, the second condition (16b) shifts the frequency range that guarantees

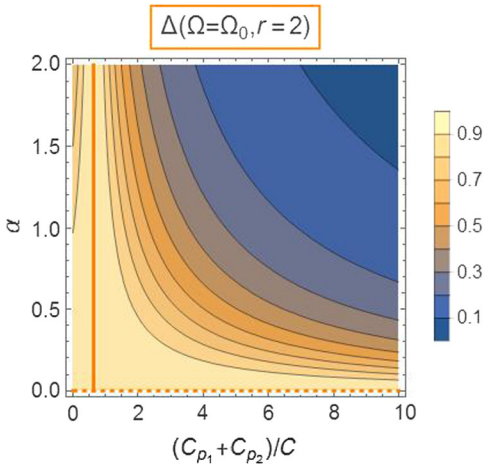

FIG. 7. Δ as a function of α and of the sum of the parasitic capacitors, normalized over $C \equiv c_1 L_1$ at $r = 2$ and at the first gyration frequency, $\Omega = \Omega_0$. Along the orange lines, $\Delta = 1$ and perfect gyration is attained. The solid line corresponds to Eq. (17), with $n = m - 1 = 0$, while the dashed line corresponds to $\alpha = 0$.

maximal nonreciprocity, and it governs the response for high-enough gyrator impedance.

To conclude the analysis of the parasitics, we examine the reflection properties of the device focusing on the case described by Eq. (16a), with $n = m - 1 = 0$. It turns out that, in this limit, Δ depends uniquely on α and on the sum of the two parasitic capacitors C_{p_1} and C_{p_2}. This dependence is shown in Fig. 7; it shows that our construction is barely influenced by reasonably small parasitics when the impedance mismatch is high enough. In particular, perfect gyration is always attained in the limit $\alpha \to 0$. Finally, it is interesting to note that when condition (16a) is satisfied, $\Delta = 1$ for all values of the mismatch parameter α when

$$\frac{C_{p_1} + C_{p_2}}{C} = \left|\pi(m-n) - \frac{\pi}{2}\right|^{-1} \tag{17}$$

and $m + n$ is odd.

III. CIRCULATOR

We can now analyze the circulator obtained by using the three-terminal gyrator in the interferometric (Hogan) construction shown in Fig. 8.

To see which details of the interferometer play a crucial role for gyration, it is useful to study what happens for an ideal gyrator, with the scattering parameters $S_{11} = S_{22} = 0$ and $S_{21} = -S_{12} = e^{i\varphi}$. The overall phase of the gyrator φ corresponds to the quantity defined in Eq. (11b) when the device is antireciprocal. It is straightforward to find that ideal circulation imposes the condition

$$e^{-i2\theta(L_B)} = \beta e^{-i2[\theta(L_A)+\theta(L_C)-\varphi]}, \tag{18}$$

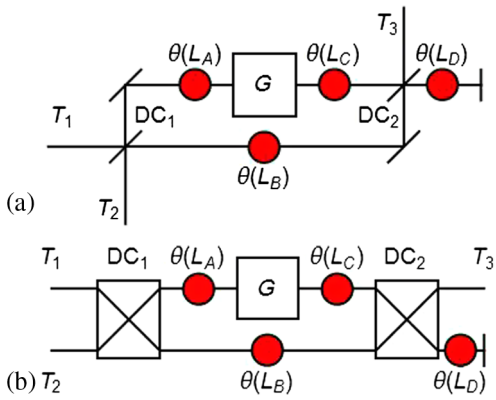

FIG. 8. Circulator construction in (a) optical and (b) microwave conventions. A standard Mach-Zender interferometer is modified by incorporating a gyrator (G) in one of the arms and by interrupting one of the arms after a directional coupler (DC) by a fully reflecting mirror, which, in microwave engineering, corresponds to either an open or a short circuit to ground. The phase $\theta(L_i)$ accumulated by a signal passing through the ith transmission line is provided by reciprocal phase shifters.

where $\theta(L_i)$ is the phase that a signal accumulates in passing through the ith lossless transmission line. For TEM modes of transmission lines, it is simply $\theta(L_i) = 2\pi L_i/\lambda$, with λ being the wavelength of the signal. The parameter β depends on the particular combination of directional couplers used: $\beta = 1$ for two equal directional couplers, and $\beta = -1$ if the directional couplers are $\pi/2$ out of phase. Moreover, when the condition (18) is satisfied, the phase $\theta(L_D)$ does not affect the absolute value of the scattering parameters, although it changes the relative phase of the signals at the different electrodes.

To have the most compact implementation of the circulator, we set $L_A = L_C = L_D = 0$, and the length L_B is then fixed by β and φ according to Eq. (18). As anticipated in Sec. II A, the overall phase of the gyrator now plays a fundamental role. Figure 9 shows how φ varies at $\Omega = \Omega_0$ as a function of r on the path defined by the ideal gyration condition (12). The overall phase varies continuously with r

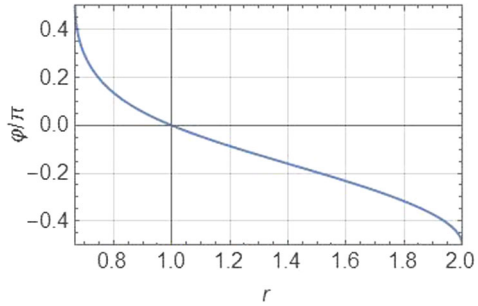

FIG. 9. Phase of the ideal HE gyrator. We focus on the first gyration frequency, $\Omega = \Omega_0$, which guarantees that φ as defined in Eq. (11a) is the actual phase of the gyrator. The plot shows φ when r and α are related by the condition (12), which corresponds to the path described by the solid orange line in Fig. 2.

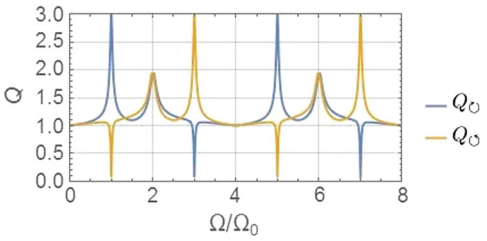

FIG. 10. $Q_{\circlearrowleft}$ and $Q_{\circlearrowright}$ as a function of Ω/Ω_0 in the most compact scenario possible, with $L_A = L_B = L_C = L_D = 0$. We use the self-matched HE gyrator with $r = 2$ and $\alpha = 0.04$, and the directional couplers are $\pi/2$ out of phase, i.e., $\beta = -1$.

from $\pi/2$ to $-\pi/2$, attaining the maximum and minimum value for the values of r corresponding to $\alpha = 0$, and it is zero for the value of r corresponding to $\alpha = 1$.

We focus on the small-α regime, with $\varphi \approx \pm\pi/2$. From Eq. (18), it easily follows that, by choosing a combination of $\pi/2$ out-of-phase directional couplers, with $\beta = -1$, good circulation is achieved with the minimal possible size, i.e., $L_B \approx 0$. In this situation, the physical scale of the circulator is determined by the gyrator and by the directional couplers. Not requiring impedance matching, the three-terminal gyrator can be made quite compact, and the main limitation on the scalability is set by the directional couplers, which typically rely on ring $\lambda/4$ resonators. Although the wavelength λ is typically a few centimeters in the microwave regime, the directional couplers can be miniaturized to λ/N, $N \approx 20$ by standard microwave-engineering tricks [14].

We now quantitatively study the performance of the quantum Hall circulator, introducing the parameters [7,13]

$$Q_{\circlearrowright} \equiv |S_{12}| + |S_{23}| + |S_{31}| \leq 3, \tag{19a}$$

$$Q_{\circlearrowleft} \equiv |S_{21}| + |S_{32}| + |S_{13}| \leq 3, \tag{19b}$$

where the equality corresponds to perfect circulation in the direction of the arrow.

We focus the analysis on the case $r = 2$, which guarantees both self-matching and tolerance against parasitics, as discussed in Sec. II. Figure 10 shows the plots of the Q parameters as a function of frequency when $\beta = -1, L_B = 0$, and $\alpha = 0.04$. It shows that excellent circulation can be attained in either direction, depending on the gyration frequency chosen. A small remark is in order here: in our model, we assume all-pass directional couplers, which is not the case for on-chip devices. However, $\lambda/4$ resonators have a bandwidth that is typically much larger than the one of the gyrator, which consequently is the main limiting factor on the frequency performance.

IV. CONCLUSION

In this study, we analyze an alternative setup for a Hall-effect gyrator. The implementation we present is experimentally easier to fabricate with respect to the previous

proposal by VD, and it exhibits a very interesting self-matching property. We predict also that this device will be, to good approximation, insensitive to parasitic coupling between electrodes. Finally, we incorporate this construction into an interferometer and verify that this setup behaves as a well-functioning circulator in an acceptable range of frequencies, and that its minimal size is limited mainly by the size of the two directional couplers.

ACKNOWLEDGMENTS

The authors would like to thank D. Reilly, A. Mahoney, A. C. Doherty, G. Verbiest, C. Stampfer, and L. Banszerus for the useful discussions. This work was supported by the Alexander von Humboldt Foundation.

APPENDIX: SCATTERING PARAMETERS

We report here the explicit expressions for the S-matrix elements in Eq. (8):

$$S_{11} = \frac{g(\Omega, r, \alpha)}{f(\Omega, r, \alpha)}, \tag{A1}$$

$$S_{21} = -\frac{4\alpha(1 - e^{i\Omega})^2}{f(\Omega, r, \alpha)}, \tag{A2}$$

with

$$f(\Omega, r, \alpha) \equiv -\alpha^2 e^{2i\Omega} + 2\alpha(\alpha+2)e^{i\Omega} - (\alpha+2)^2 + \alpha^2 e^{ir\Omega} + (\alpha-2)^2 e^{i(r+2)\Omega} - 2\alpha(\alpha-2)e^{i(r+1)\Omega}, \tag{A3}$$

and

$$g(\Omega, r, \alpha) \equiv \alpha^2(-e^{ir\Omega} + 2e^{i(r+1)\Omega} - 2e^{i\Omega} + e^{2i\Omega}) + (\alpha^2 - 4)(1 - e^{i(r+2)\Omega}). \tag{A4}$$

[1] D. Ristè, C. C. Bultink, K. W. Lehnert, and L. DiCarlo, Feedback Control of a Solid-State Qubit Using High-Fidelity Projective Measurement, Phys. Rev. Lett. **109**, 240502 (2012).

[2] J. M. Chow, J. M. Gambetta, E. Magesan, D. W. Abraham, A. W. Cross, B. R. Johnson, N. A. Masluk, C. A. Ryan, J. A. Smolin, S. J. Srinivasan, and M. Steffen, Implementing a strand of a scalable fault-tolerant quantum computing fabric, Nat. Commun. **5**, 4015 (2014).

[3] C. L. Hogan, The ferromagnetic Faraday effect at microwave frequencies and its applications: The microwave gyrator, Bell Syst. Tech. J. **31**, 1 (1952).

[4] C. L. Hogan, The ferromagnetic Faraday effect at microwave frequencies and its applications, Rev. Mod. Phys. **25**, 253 (1953).

[5] D. F. Berndt and S. C. Dutta Roy, Inductor simulation using a single unity gain amplifier, IEEE J. Solid-State Circuits **4**, 161 (1969).

[6] D. M. Pozar, *Microwave Engineering*, 4th ed. (Wiley, New York, 2011).

[7] G. Viola and D. P. DiVincenzo, Hall Effect Gyrators and Circulators, Phys. Rev. X **4**, 021019 (2014).

[8] R. F. Wick, Solution of the field problem of the germanium gyrator, J. Appl. Phys. **25**, 741 (1954).

[9] R. W. Rendell and S. M. Girvin, Hall voltage dependence on inversion-layer geometry in the quantum Hall-effect regime, Phys. Rev. B **23**, 6610 (1981).

[10] A. C. Mahoney, J. I. Colless, S. J. Pauka, J. M. Hornibrook, J. D. Watson, G. C. Gardner, M. J. Manfra, A. C. Doherty, and D. J. Reilly, On-Chip Microwave Quantum Hall Circulator, Phys. Rev. X **7**, 011007 (2017).

[11] H. J. Carlin, in *Proceedings of the Symposium on Modern Advances in Microwave Techniques*, edited by J. Fox (Brooklyn Polytechnic Institute, 1955), p. 175.

[12] H. J. Carlin and A. B. Giordano, *Network Theory: An Introduction to Reciprocal and Non-reciprocal Circuits* (Prentice-Hall, Englewood Cliffs, NJ, 1964).

[13] B. Placke, S. Bosco, and D. P. DiVincenzo, A model study of present-day Hall-effect circulators, arXiv: 1609.09624 [EPJ Quantum Technology (to be published)].

[14] R. N. Simons, *Coplanar Waveguide Circuits, Components, and Systems*, Vol. 165 (Wiley, New York, 2004).

[15] M. E. Cage, K. von Klitzing, A. M. Chang, F. Duncan, M. Haldane, R. B. Laughlin, A. M. M. Pruisken, D. J. Thouless, R. E. Prange, and S. M. Girvin, *The Quantum Hall Effect* (Springer Science+Business Media, Berlin, 2012).

[16] S. Bosco and D. P. DiVincenzo, Non-reciprocal quantum Hall devices with driven edge magnetoplasmons in 2-dimensional materials, arXiv:1701.08448.